Response to Editor

Dear Editor,

our point-by-point response to the reviews is uploaded to

http://www.atmos-chem-phys-discuss.net/14/C12530/2015/acpd-14-C12530-2015-supplement.pdf

and it is also attached to this document.

A list of all relevant changes is attached as well as a marked up version of the manuscript.

We think, that both anonymous Referees contributed a very constructive review as we were able to perform substantial improvements to the manuscript in response to all major points of criticism.

We hope our paper is now mature for final publication.

Thanks for your efforts.

Sincerely,

Hannes Vogelmann

FINAL RESPONSE, H. VOGELMANN, KARLSRUHE INSTITUTE OF TECHNOLOGY, IMK-IFU, GARMISCH-PARTENKIRCHEN, GERMANY, MARCH 6, 2015

We thank both anonymous referees for their very sound and constructive comments which helped to significantly improve our manuscript. We thereafter present our point to point reply.

Referee #1, General comments:

> 1. The conclusions related to the statistics presented in Figures 3, 4, and 5 are de- pending also on the number of sampling cases. For example, in figure 3, both for the curves investigating the variability of the integrated water vapor (IWV) as a function of the horizontal distance x between the center of gravity of FTIRIWV and DIAL IWV in summer and winter, the change in the slope of the curves showing a change in the IWV variability is also corresponding to a decrease in the number of cases available for the analysis. Is in this cases the sampling sufficient to justify your conclusion? The minimal sampling issue in your analysis should discussed and justifies to ultimately support you conclusions. This is important not only to justify the reliability of your analysis but also to assess the real magnitude of the IWV variability with the change of the time and vertical resolution, the seasons, and any other relevant parameters to correlate with the IWV.

Thank you for this helpful comment. Of course, the standard deviation of the differences between IWV samples from FTIR and DIAL can be considered as measurement with an uncertainty. This uncertainty partly depends on the number of samples respected for the calculation. Because of the small sample-sizes we decided to use the bias-corrected estimate S(s) = s / sqrt (2 (n-1)). We added the uncertainty as error bars in Figs. 3-5 and added information to the figure captions and also 2 sentences in the text.

> 2. From the text of the manuscript, it seems that the aim is also to provide a more general methodology to assess the uncertainty due to the non-physical collocation of atmospheric measurements: this should be better explained since the generalization of this approach to other sites and instruments, as suggested in the conclusions, looks extremely depending of the experimental setup of the lidar and FTIR and the Zugspitze site. Possible extension and limits of the methodology should be clearly identified and discussed.

Our analysis is mostly applicable to the free troposphere. However, it is a consequence of measuring above a complex alpine terrain that we observe the influence of local convection in our measurement range during the warm season (up to 4 - 4.5 km). Our results show, that the amplitudes of the water vapor variability induced by long-range transport can exceed those induced by local convection by roughly one order of magnitude. From this, one could conclude, that the variability inside the boundary layer above less complex terrain, is assumably reduced to values that we observe under stable conditions with local convection reaching our measurement range and dominating the observed variability. This assumption, of course, implies that the fast advection of heterogeneous air layers does not impact the boundary layer. We added this thought to the conclusions.

> 3. The analysis reported in sections 4 and 5 related to the water vapor variability alone the vertical profiles might be strongly enhanced by the use of data from mesoscale models in support of the air mass backtrajectory analysis alone. Moreover, more details about the backtrajectory analysis should be included like if an isentropic or a vertical velocity model has been considered to run Hysplit. Indeed, backtrajetories could be reported below each of the figure 8-11.

For the two cases of local convection we find that backward

trajectories do not yield much helpful input, because the observed variability was initiated locally. The calculated trajectories in principle describe the atmospheric conditions. Downwelling in the stable case and upwelling in the unstable case. Also mesoscale models do not resolve the details of these very local processes better than our direct visual (and lidar) observations of local slope updrifts or the nearby formation of a thunderstorm. Thus, we added only a descriptive sentence.

For the stratospheric intrusion case we decided to show one trajectory plot from ETH Zuerich calculated with the Lagrangian model "LAGRANTO". One reference added. This trajectory model provides potential vorticity and is well suited for studies of stratosphere to troposphere transport. The spaghetti plot shows the particular complex dynamic of this event.

For the second long-range transport case, we added two HYSPLIT trajectory plots which show a switching between Pacific surface-level and Pacific upper troposphere as very remote source regions.

Referee #1, Specific comments:

>1. page 8, lines 9-10: the difference in the typical time
>integration used for the lidar and the FTIR should be justified and
>the authors should explain if and how this may impact the analysis.

The integration times are inherent for both DIAL and FTIR and are needed to achieve reasonable SNR values. But, of course, they tend to blur out very short-term variations on the minute scale. The difference of 13 to 17 minutes mean that the DIAL underestimates very short term variability of IWV a little more than the FTIR. For our variability analysis the integrations times mean, analogously to error propagation that single variations within a time of less than 4 minutes are statistically underestimated by a factor of about 2. Two sentences added.

> 2. page 8, lines 23-25, the statement at the point number 2 about
> the heat driven convective dynamic should be supported by a
> reference or a previous study.

Convection being stronger during the summer season is generally accepted. 2 references to former studies are added.

> 3. page 8, lines 26, why did the authors use measurements pairs
> within different time intervals in winter and summer? Is this
> related to the IWV variability? Please clarify.

See answer to comment 3 by Referee #2.

> 4. page 10, lines 2-6: indeed, the minimum average distance is
> something like 50 days far from the maximum variability of the
> water vapor. This means that this conclusion is a bit forced and
> should be reconsidered.

Thanks for this comment. Statement is modified.

> 5. page 11, lines 5-10: also in this case the conclusion is a bit
> forced and should be reconsidered. The blue and red curves start
> being divergent above 30 minutes, though in a less pronounced way
> than below 30 minutes.

By mistake, the submitted Fig. 5 was a very old and preliminary version based on a deficient data-filtering. It is replaced and now supports our conclusions much better.

> 6. Since the manuscript aims at assessing collocation uncertainty

> too, the errors bars dealing with the random and bias component of
> the uncertainty should be reported everywhere in the plots to
> support the discussion.

Done so. See comment 4, Referee #2.

> 7. Conclusion should be reconsidered according to the general
> comment #2.

Done so, see comment #2.

Referee #1, Technical corrections:

> 1. y-axis label in figures 8-11 should report altitude above
> ground or sea level.

Done so.

> 2. page 4, line 1: "at our site" please change it in "at Zugspitze
> site".

Done so, and also at some other places.

> 3. page 5, line 19: please replace examining for example with
> investigating.

Done so.

> 4. page 7, lines 15-19: please rephrase, I got the meaning but the
> sentence is some- how cryptic.

Sentence added.

> 5. Figures 3-5, not sure the number on the plots are the best way
> to consider the data sampling maybe the authors could couple
> number and colors, though this is only an advise not mandatory.

After many attempts to make these figures as readable as possible we came to the result, that writing numbers beside the curves is best. For assigning the numbers to their related curve we plotted them in the same color for Figs. 3-5.

Referee #2 General comments:

> Specific comments: 1. Provide defining equations for the
> statistical quantities used, and describe in more (mathematical)
> detail how they are determined. It is quite an effort to come up
> with a consistent set of equations, but it would take the
> guesswork out of the paper.

We agree with this point and explain the mathematical retrievals for statistical quantities in more detail. In fact, the retrieval is a bit more sophisticated, than just calculating the standard deviation of differences between the IWV values from both instruments: simga_IWV is the standard-deviation of IWV residuals from a linear model which is given by a regression line calculated for each sample. However, for large sample sizes (n > 20) this yields almost equal results as just calculating SDD between the IWV-values from DIAL and FTIR themselves. Therefore, we added information about this to Sect. 3.

> 2. The authors use the center of gravity height of the vertical
> water-vapor distribution to define the reference plane in which
> the distance between FTIR measurement and DIAL measurement is
> computed. Further, they state that the FTIR measures (IWV of) the
> vertical water-vapor distribution, at least that¿s how the
> reviewer understands the caption of Fig. 1. That¿s confusing. The
> FTIR certainly does not measure vertical IWV but IWV along a

> slanted path. So is an air mass factor taken into account in the
> FTIR retrieval to provide IWV? Please clarify.

Of course, vertical profiles and IWV values from the FTIR instrument are calculated with an angle correction to be consistent with vertical pointing. To clarify this, a sentence is added to Sect. 2.1 and modified the caption of Fig. 1.

> 3. Running text (pp. 8,9) and caption of Fig. 3 are contradictory.
> Is the coincidence time interval 60 min for both winter and summer
> data sets (see caption), or only for the winter data set (and 30
> min for summer, see text)? Please, check! If data shown in Fig. 3
> are indeed for 60 min in both cases, why not show 60-min points in
> Fig. 2?

Thank you for this comment. In a first attempt we used a coincidence interval of 30 minutes for both summer and winter. Because of low sample sizes for larger distances, we switched to 60 minutes, but only for the winter season. We corrected this in the caption of Fig. 3. If using 60 minutes also for summer, the clear onset of the spatial fraction of the variability slightly blurs out.

> 4. Measurements have errors. Some more comments on the robustness
> of the retrieval would be appreciated. At the very least include
> error bars in Figs. 8-11.

We added error bars to Figures 8-11. And added some information about the robustness of the retrieval and error considerations to the text.

> 5. Are the backtrajectory computations reliable enough to trace
> back the origin of the air masses to the North-West Pacific Ocean?
> How many days backwards? The results are plausible, but. . .

In principle, back trajectories are not considered as proof, but for plausibility. Backtracking more than 10 days, of course, is not always reliable. For the North-West-Pacific case, we took this just as basic information of possible origins and than looked at weather charts and satellite images of this region. We added trajectory plots with some comments. See also comment 3 by Referee #1.

Referee #2, Technical corrections:

>Some typos: 1. P. 5, l. 9: ¿information¿

Done.

> 2. P. 15, l. 12: explain "Alpine pumping"

Done.

> 3. P. 16, l. 16: "these conditions"

Done.

> 4. P. 19, l. 20: "relative short-term" or "relatively short-term"?

Changed to relative 'short-term'.

> 5. P. 36, l. 2: unit "s" not in italic

Done.

Page : 3 Line : 116 Author : Hannes Vogelmann 02/09/2015
Refers to Referee #2, comment 2.

Page : 3 Line : 134 Author : Hannes Vogelmann 02/02/2015
Refers to Referee #2, comment 4.

Page : 4 Line : 159 Author : Hannes Vogelmann 03/03/2015
Added due to comment T4, Referee #1.

Page : 5 Line : 183 Author : Hannes Vogelmann 03/02/2015
Added to makes things more clear, due to comment 1, Referee #2

Page : 5 Line : 196 Author : Hannes Vogelmann 02/09/2015
Added equations and text due to comment 1 by Referee # 2.

Page : 5 Line : 201 Author : Hannes Vogelmann 03/02/2015
Added information about uncertainty and reliability in context with the sample size, as requested by Referee #1, comment 1.

Page : 5 Line : 204 Author : Hannes Vogelmann 03/02/2015
Added comment about instrument integration times as requested by comment s1, Referee# 1

Page : 6 Line : 217 Author : Hannes Vogelmann 03/02/2015
Sentence and References added due to comment s2, Referee #1.

Page : 6 Line : 252 Author : Hannes Vogelmann 03/02/2015
Modiefied due to comment s4, Referee #1.

Page : 6 Line : 255 Author : Hannes Vogelmann 03/02/2015
Sentence added due to comment s4, Referee #1.

Page : 9 Line : 366 Author : Hannes Vogelmann 03/03/2015
Added due to comment 3, Referee #1.

Page : 9 Line : 372 Author : Hannes Vogelmann 03/03/2015
Added due to comment 5, Referee #2.

Page : 10 Line : 406 Author : Hannes Vogelmann 03/03/2015
Added due to comment t2, Referee #2.

Page : 10 Line : 425 Author : Hannes Vogelmann 02/25/2015
Refers to comment 3, Referee #1.

Page : 11 Line : 452 Author : Hannes Vogelmann 02/25/2015
Refers to comment 3, Referee #1

Page : 11 Line : 464 Author : Hannes Vogelmann 02/25/2015
Refers to comment 3, Referee #1

Page : 13 Line : 547 Author : Hannes Vogelmann 02/25/2015
Refers to comment 2, Referee #1.

Page : 18 Line : 788 Author : Hannes Vogelmann 03/06/2015
Reference added, due to model used for the trajectory plot in new Fig. 11

Page : 19 Line : 815 Author : Hannes Vogelmann 02/09/2015
Added due to Referee #2, comment 2.

Page : 21 Line : 828 Author : Hannes Vogelmann 02/02/2015
Error bars added due to comment 1 of Referee #1.

Page : 21 Line : 836 Author : Hannes Vogelmann 02/09/2015
Refers to Referee #2, comment 3.

Page : 22 Line : 847 Author : Hannes Vogelmann 02/02/2015
Error bars added due to comment 1 of Referee #1.

Page : 23 Line : 866 Author : Hannes Vogelmann 02/02/2015
Error bars added due to comment 1 of Referee #1.

Page : 26 Line : 898 Author : Hannes Vogelmann 02/02/2015
Error bars added due to comment 4 of Referee #2.

Page : 27 Line : 916 Author : Hannes Vogelmann 02/02/2015
Error bars added due to comment 4 of Referee #2.

Page : 28 Line : 937 Author : Hannes Vogelmann 02/02/2015
Error bars added due to comment 4 of Referee #2.

Page : 29 Line : 957 Author : Hannes Vogelmann 02/25/2015
Added Figure as suggested by comment 3, Referee #1.

Page : 30 Line : 967 Author : Hannes Vogelmann 02/02/2015
Error bars added due to comment 4 of Referee #2.

Page : 31 Line : 1016 Author : Hannes Vogelmann 02/25/2015
Added Figure as suggested by comment 3, Referee #1,Last sentence refers to comment 5, Referee #2.

Spatio-temporal variability of water vapor investigated by lidar and FTIR vertical soundings above Mt. Zugspitze

H. Vogelmann, R. Sussmann, T. Trickl, A. Reichert

Karlsruhe Institute of Technology, IMK-IFU, Garmisch-Partenkirchen, Germany

Abstract: Water vapor is the most important greenhouse gas and its spatio-temporal variability by far exceeds that of all other greenhouse gases. However, water vapor variability has hardly been studied quantitatively so far. We present an analysis of a five-year period of water vapor measurements in the free troposphere above Mt. Zugspitze (2962 m a.s.l., Germany). Our results are obtained from a combination of measurements of vertically integrated water vapor (IWV), recorded with a solar Fourier Transform InfraRed (FTIR) spectrometer on the summit of Mt. Zugspitze and of water vapor profiles recorded with the nearby differential absorption lidar (DIAL) at the Schneefernerhaus research station. The special geometrical arrangement of one zenith-viewing and one sun-pointing instrument and the temporal resolution of both instruments allow for an investigation of the spatio-temporal variability of IWV on a spatial scale of less than one kilometer and on a time scale of less than one hour. The standard deviation of differences between both instruments σ_{IWV} calculated for varied subsets of data serves as a measure of variability. The different subsets are based on various spatial and temporal matching criteria. Within a time interval of 20 minutes, the spatial variability becomes significant for horizontal distances above 2 km, but only in the warm season (σ_{IWV} = 0.35 mm). However, it is not sensitive to the horizontal distance during the winter season. The variability of IWV within a time interval of 30 minutes peaks in July and August (σ_{IWV} > 0.55 mm, mean horizontal distance = 2.5 km) and has its minimum around midwinter (σ_{IWV} < 0.2 mm, mean distance > 5 km). The temporal variability of IWV is derived by selecting subsets of data from both instruments with optimal volume matching. For a short time interval of 5 minutes, the variability is 0.05 mm and increases to more than 0.5 mm for a time interval of 15 hours. The profile variability of water vapor is determined by analyzing subsets of water vapor profiles recorded by the DIAL within time intervals from 1 h to 5 h. For all altitudes, the variability increases with widened time intervals. The lowest relative variability is observed in the lower free troposphere around an altitude of 4.5 km. Above 5 km, the relative variability increases continuously up to the tropopause by about a factor of 3. Analysis of the covariance of the vertical variability reveals an enhanced variability of water vapor in the upper troposphere above 6 km. It is attributed to a more coherent flow of heterogeneous air masses, while the variability at lower altitudes is also driven by local atmospheric dynamics. By studying the short-term variability of vertical water vapor profiles recorded within a day, we come to the conclusion that the contribution of long-range transport and the advection of heterogeneous layer structures may exceed the impact of local convection by one order of magnitude even in the altitude range between 3 km and 5 km.

1. Introduction

Water vapor plays a key role in weather and climate phenomena and is the most important greenhouse gas (e.g. Harries, 1997; Kiehl and Trenberth, 1997; Trenberth et al., 2007). However, the feedback between the anthropogenic (CO_2-driven) temperature increase and the influence of water vapor is far from being understood (e.g. Wagner et al., 2006). Furthermore, climate

projections still suffer from inaccurate parameterizations of water vapor absorption processes within the radiation code of general circulation models (e.g. Turner and Mlawer, 2010). Understanding the role of water vapor in the climate system is particularly complex, because water vapor is the only trace compound in the atmosphere showing up in all three states of matter. This has a variety of implications, e.g. the possibility of transporting latent heat (thereby damping latitudinal temperature gradients) or the fact that precipitation is the largest sink of atmospheric water vapor. The latter is the main reason of the strong decrease of water vapor concentration with altitude, and it is the reason why water vapor has an average lifetime in the atmosphere of just about 9 days, which is shorter than for any other greenhouse gas. This results in the very high spatio-temporal variability of water vapor (Trenberth, 1998).

However, the spatio-temporal variability of water vapor on the scales relevant to weather and climate is still far from being quantitatively characterized, and the underlying processes are not well understood. Variability, for instance, may be caused by local dynamics above complex mountain terrain (which changes with season), by regional meteorological effects, or by the advection on larger scales. A highly interesting question is the variance of water vapor as a function of altitude on different time scales. Previous studies based on ozone and aerosol lidar profiling demonstrated that the free troposphere may be affected by regional contributions, long-range transport, and stratosphere-troposphere exchange causing strongly and rapidly changing vertical structures in the concentration profile (Eisele et al., 1999; Stohl and Trickl, 1999; Trickl et al., 2003; Trickl et al., 2010; Trickl et al., 2011). In particular, we frequently observed very dry and sometimes very thin layers in the free troposphere, which were associated with stratospheric intrusion events. It is still unclear, however, whether such processes significantly contribute to the observed variability of water vapor in the middle and upper troposphere.

For understanding the long-term changes and the variability of water vapor, high-quality vertical sounding of water vapor with high temporal density is required. During the past years, a variety of optical remote sounders have been developed for this purpose in addition to the classical radiosondes (e.g. Kämpfer, 2013). Lidars, Fourier-transform-infrared (FTIR) spectrometers, and microwave radiometers fulfill the requirements of frequent measurements. In particular, we developed a differential absorption lidar (DIAL) for use at Mt. Zugspitze, which allows for continuous day- and nighttime soundings of water vapor profiles up to the tropopause (Vogelmann and Trickl, 2008).For measuring integrated water vapor (IWV), the solar FTIR technique was found to be one of the most accurate and precise ground-based sounding techniques with a precision better than 0.05 mm (1.7 % of the mean; Sussmann et al., 2009). According to a recent validation study, these lidar and FTIR water vapor sounders are in excellent agreement (Vogelmann et al., 2011).

Comparing two high-precision state-of the art water vapor sounders, we also found that it is necessary to use very strict temporal coincidence criteria on the time scale of minutes and a spatial matching on the scale of 100 m. Otherwise, the combined precision of the instruments will be affected by the natural variability of water vapor (Sussmann et al., 2009; Vogelmann et al., 2011). This was confirmed by Bleisch et al. (2011), who reported that in case of long distances between the locations of the intercompared instruments, atmospheric variability tends to blur out the significance of validation results. The question of co-location has also become an issue in the Global Climate Observing System (GCOS) Reference Upper Air Network (GRUAN) (Immler et al., 2010; Sun et al., 2010; Seidel et al., 2011, Fasso et al., 2014) and it was addressed when evaluating water vapor sounding validation campaigns like MOHAVE (2009), LUAMI (2008), WAVES (2006), AWEX-G (2003) (Leblanc et al., 2011; Stiller et al., 2012; Wirth et al., 2009; Adam et al., 2010; Whiteman et al., 2006). Co-location also is of relevance to ground-based

validation of satellite missions and has been addressed many times (e.g., Tobin et al., 2006, Soden and Lanzante, 1996).

The goal of this paper is to derive quantitative information relating to the spatio-temporal variability of water vapor. Using the solar FTIR spectrometer on the summit of Mt. Zugspitze (2962 m a.s.l.,) and the DIAL located only 680 m to the southwest and about 288 m below the summit, the unique geometrical arrangement of two high-precision water vapor sounders allows for an advanced analysis of the spatio-temporal variability of integrated water vapor (IWV) on small scales (Δt < 1 h, Δx < 1 km).

After a brief description of the instrumental setup as well as of the FTIR and DIAL IWV data with their geometrical and temporal properties, we present the quantification of the spatial and temporal variability of IWV by a statistical analysis of selected subsets of IWV data from the FTIR and the DIAL (Sects 3.1 and 3.2). The profile-type variability of the vertical water vapor distribution is analyzed quantitatively by investigating~~examining~~ selected subsets of DIAL soundings and by calculating a profile covariance matrix (Sect. 4). Different mechanisms driving the short-term variability of water vapor are investigated in four case studies (Sect. 5). Finally, major results are summarized (Sect. 6).

2 Instrumentation and geographical arrangement

2.1 Zugspitze solar FTIR system

Solar absorption FTIR spectrometry uses the direct radiation from the sun in the mid-infrared range as a light source. The FTIR provides total columns of numerous atmospheric trace gases. Additionally, information on the vertical distribution of trace gases can be derived (typically 2-3 degrees of freedom in a retrieval optimized for IWV) from the shape of the pressure-broadened infrared lines. Due to its principle, the solar FTIR is pointing towards the actual position of the sun and measures slant columns/profiles ~~pointing towards the actual position of the sun~~.that are angle corrected for consistence with vertical profiles. The FTIR instrument located on the summit of Mt. Zugspitze is based on a Bruker IFS125HR interferometer and is described in detail by Sussmann and Schäfer (1997, Table 1). The retrieval of IWV is based on the SFIT 2 algorithm (Pougatchev et al., 1995), which is the standard code of the Network for the Detection of Atmospheric Composition Change (NDACC). An FTIR retrieval optimized for IWV was developed recently by Sussmann et al. (2009). The precision of IWV retrieval was estimated to be better than 0.05 mm (2.2 % of the mean).

2.2 Differential Absorption Lidar (DIAL)

DIAL is a laser-based remote sensing technique providing number-density profiles of trace gases. Measurements are based on the specific molecular absorption of the gases and the well-established spectroscopy. The Zugspitze DIAL is operated with single absorption lines in the 817-nm band of H_2O (Table 2) for ground-based water vapor profiling in the free troposphere. In order to keep a balanced signal-to-noise ratio a vertical resolution (VDI Guideline 4210) of 50 m to 300 m is adapted dynamically to the vertical range from 2.95 km to roughly 12 km a.s.l., respectively. Thus, statistical measurment uncertainties are kept below about 5% related to a mean humidity profile throughout the free troposphere. The sensitivity limit is roughly 18 ppm at 10 km a.s.l. which can occasionally be undercut in the upper troposphere. If this ist the case, the upper end of the valid measurement range is reasonably reduced to lower altitudes. Statistical measurement uncertainties are given by error bars (+- 2σ) in Figs. 8-11. The DIAL instrument is located at the Schneefernerhaus research station (UFS) on the steep southern slope of Mt. Zugspitze at an altitude of 2675 m a.s.l.. The range of the Zugspitze DIAL starts 250 m above the laboratory, slightly below the altitude of the FTIR spectrometer. The DIAL system at

Schneefernerhaus / Zugspitze and the retrieval of water vapor profiles are described in more detail by Vogelmann and Trickl (2008). Water vapor profiles from the Zugspitze DIAL IWV with a precision better than 0.1 mm (Vogelmann et al., 2011).

Table 1: Specifications of the FTIR and the DIAL on Mt. Zugspitze

	FTIR	DIAL
Geographical coordinates	E 10°59'8.7" N 47°25'15.6"	E 10°58'46.8" N 47°25'0"
Altitude a.s.l.	2964 m	2675 m
Vertical range a.s.l.	above 2.96 km	2.95 km - 12 km
Typ. integration time	13.3 min	17 min
Spectral range [cm^{-1}]	micro windows	ν_{on}
	839.5 – 840.5	12236.560
	849.0 – 850.2	12237.466
	852.0 – 853.1	12243.537

2.3 Geographical setup and IWV data selection

The Zugspitze (47.42°N, 10.98°E, 2962 m a.s.l.) is by far the highest mountain on the northern rim of the Alps. The free troposphere above this site is representative of Central Europe. The mountain is above the moist boundary layer for most of the year. Due to reduced absorption losses, this site is ideal for sensitive spectroscopic measurements of water vapor throughout the free troposphere. While the FTIR instrument is located on the summit of Mt. Zugspitze, the DIAL instrument is located at the Schneefernerhaus research station (UFS) on the steep southern slope of Mt. Zugspitze at an altitude of 2675 m a.s.l., 680 m southwest of the FTIR instrument (see Fig. 1).The sun-pointing geometry of the FTIR instrument and the fixed zenith-pointing geometry of the DIAL allow for studies of the differences of IWV values measured by both instruments with a defined spatial and temporal matching (Fig. 1). According to reanalysis data from the National Center for Environmental Prediction (NCEP), the center of gravity of the water vapor vertical distribution above Mt. Zugspitze most frequently is located at a rather constant altitude between 4300 m a.s.l. in summer and 4400 m a.s.l. in winter. For simplicity, it is assumed that the FTIR IWV is horizontally located at the point where the viewing direction of the instrument meets the altitude level of the center of gravity of the IWV distribution. This assumption, of course, describes the reality at high sun elevation angles better while the measured FTIR IWV~~,~~ is more horizontally blurred for low sun elevations close to the horizon. From this and the actual position of the sun, a rough estimate of the varying horizontal position of the IWV measured by the FTIR instrument is possible. The zenith angle of the sun defines the horizontal distance from the instrument, which may vary from less than 1 km around noon in midsummer to more than 10 km at very low sun positions. The azimuth of the FTIR IWV position is equal to the azimuth of the sun position, which depends on daytime and season. In contrast to this, the horizontal position of IWV measured with the DIAL is always fixed to the location of the instrument, 680 m southwest of the FTIR site. This is illustrated in Fig. 1.

Figure 2 shows the horizontal allocation of all FTIR IWV measurements recorded in coincidence ($\Delta t \leq 30$ min) with a DIAL measurement. The horizontal distance between the location of the DIAL and the horizontal position of the IWV measured by the FTIR is defined as spatial matching Δx. Figure 2 also shows the daily trajectories of the horizontal position of the center of gravity of IWV probed with the FTIR instrument for midsummer, equinox, and

midwinter. In the summer season, the mean horizontal distance Δx is obviously smaller than during winter (see also dashed curve in Fig. 4).

3 Variability of integrated water vapor in space and time

Of the more than 350 lidar profiles recorded in the years 2007-2009, more than 250 profiles were measured during daytime (i.e. between 5h00 and 19h00 local time). In the same period, more than 3500 column measurements were made by the FTIR instrument. Both systems operate with a typical integration time of 13 min (FTIR) and 17 min (DIAL). In order to obtain a quantitative measure of the water vapor variability, we analyzed certain measurement samples recorded by the two different instruments under certain spatio-temporal matching criteria for Δx and Δt. The center of the integration time of FTIR and DIAL each was used to determine the temporal matching. We retrieved σ_{IWV} by calculatinge the standard deviation of the differences of IWV values from a linear modell y = a*x +b:~~σ_{IWV} between the IWV values.~~

$$\sigma_{\mathrm{IWV}} = \sqrt{\frac{1}{n-2}\sum_{i=1}^{k}(y_i - (ax_i + b))^2}$$

whereat y_i and x_i are the IWV-values from the DIAL and the FTIR, respectively, within one sample and n is the sample size. *a* and *b* were calculated by a regression analysis using the method of least squares. Thus,

$$\sigma_{\mathrm{IWV}} = \sqrt{\frac{1}{n-2}\sum_{i=1}^{n}\left(y_i - \bar{y} - \frac{(x_i - \bar{x})\sum_j (x_j - \bar{x})y_j}{\sum_j (x_j - \bar{x})^2}\right)^2}$$

~~recorded by the two different instruments under certain spatio-temporal matching criteria Δx and Δt.~~ The matching criteria amongst others define the sample size *n*, which influences the uncertainty of σ_{IWV} itself. The uncertainty of σ_{IWV} is given by σ_{IWV} / sqrt(2(*n*-1)) and illustrated by the error bars in Figs. 3-5. The inherent integration times of the instruments (roughly 15min) cause a statistical underestimation of short term variabilities on the minute scale. For the shortest time intervals investigated here (4 min), variations are statistically underestimated by factor of about 2.

3.1 Spatial variability

We decided to analyze the spatial and temporal variabilities separately for summer and winter because of two counteracting effects:

1. The special observation geometry in this study implies that the spatial overlap Δx of both soundings depends on both daytime and season. As shown in Figs. 1, 2, and 4 (dashed curve), the best spatial matching ($\Delta x < 1$ km) is achieved around midsummer in the early afternoon only (between 12 h and 14 h UTC), while Δx is always larger during the winter season.

2. Due to heat-driven convective dynamics in complex mountain surroundings, spatial and temporal variabilities of IWV are expected to be higher during summer season. The convection

above alpine terrain can reach an altitude of about 1.5 km above the mean summit levels in summer (Carnuth 2000, Kreipl 2005). During all other seasons, the convection usually does not even reach the Zugspitze summit and our measurement range.~~and lower during winter~~.

For determining the spatial variability of IWV, we calculated σ_{IWV} as a function of varied spatial matching Δx by using measurement pairs within a time interval of Δt = 30 min (summer) and Δt = 60 min (winter). As mentioned above, it was shown that for a good agreement of both systems very tight spatial and temporal matching criteria are mandatory (Vogelmann et al., 2011).

Figure 3 (red curve) shows σ_{IWV} as a function of the horizontal distance of the probed volumes in the summer season. While σ_{IWV} constantly remains around 0.35 mm for Δx < 2 km, it rises to values of more than 0.65 mm at a distance of Δx = 4 km. This result shows that the variability depends on the spatio-temporal matching. Up to Δx = 2 km, the temporal variability within the selected time interval (Δt = 30 min) predominates. For larger distances, the contribution of spatial variability becomes significant.

In contrast to this, σ_{IWV} is not increasing with Δx in the winter season (Fig. 3, blue curve). This is in agreement with the assumption that local convection does not reach the vertical measurement range during the winter season and that the IWV variability is probably dominated by horizontal advection of filamentary structures in the free troposphere from very different source regions. Consequently, the observed variability during winter is due to larger spatial scale processes (compared to local convection in summer), which would explain the absence of an increase with Δx in Fig. 3. Note that because IWV is much lower in winter than in summer, the relative variabilities (i.e. if σ_{IWV} were given in per cent) would be larger for the blue curve in Fig. 3. This means that advection of filaments (winter) leads to larger relative changes of IWV than local convection in summer. We will discuss this finding in more detail within the context of the variability of the vertical water vapor profile in Sect. 4. Figure 3 also indicates that σ_{IWV} even shows a trend to lower values for distances above 6 km. We explain this by the fact that measurements with large horizontal mismatch (Δx > 6 km) require extraordinarily calm and clear weather conditions, because the FTIR instrument requires a cloudless field of view and the sun position already close to the horizon.

Figure 4 shows σ_{IWV} as a function of the Julian day. Here, counteracting effects can be observed. While the mean horizontal distance (dashed curve) is low in the summer season (Δx < 2 km), it reaches up to almost 10 km around midwinter. The variability over the entire field of horizontal distances within a certain time interval (e.g. 20 min) reaches its maximum of almost 0.6 mm when the temperature peaks around the end of July. We assume that this is a direct effect of the heat-driven local convection, which can reach altitudes of 4.5 km at ~~our~~Zugspitze site during the summer season (Reiter et al., 1983; Müller and Reiter, 1986; Carnuth and Trickl, 2000; Carnuth et al., 2002; Kreipl, 2005). The fact that the ~~maximum~~ variability shows moderate values at the ~~is found close to~~ the minimum average distance~~-~~ leads to the assumption that ~~the former~~ it is partially caused by local effects. As expected, ~~T~~the minimum variability of about 0.15 mm is observed around midwinter when temperatures are low, although the mean horizontal mismatch of both instruments is largest at this time of the year. This supports the assumption that local dynamics do not play a significant role during midwinter.

3.2 Temporal variability

For the analysis of temporal variability, we calculated the standard deviation of differences σ_{IWV} between IWV values from both instruments as a function of temporal coincidence. This was repeated for varied spatial matching criteria.When using all IWV values from both instruments without applying any geometrical matching criteria, σ_{IWV} shows a flat minimum around a coincidence interval of Δt = 20 min, see red curve in Fig. 5. About 100 – 300 coincident pairs

contribute to the ensembles within this minimum. At first, a minimal σ_{IWV} for the shortest interval length would be expected. Two different effects are responsible for the minimum around Δt = 20 min. First of all, most FTIR and lidar measurements were made in the morning, because there are still few clouds. As a consequence, most of the pairs with the shortest coincidence intervals are found in the morning where the spatial matching is worst (see Figs. 1 and 2). This slightly increases σ_{IWV} on the very left hand side of the red curve in Fig. 5. Secondly, many pairs with good spatial matching can be found around noon, even for somewhat larger temporal coincidence intervals. This explains the decrease of sigma IWV towards the minimum (red curve in Fig. 5).

When considering measurement pairs with an FTIR sun azimuth close to the position of the DIAL instrument (210° ± 6°) only, σ_{IWV} is much smaller in general and has its minimum at the shortest coincidence intervals (green curve in Fig. 5). For time intervals on the minutes scale, we find σ_{IWV} = 0.05 mm, which agrees with the validated (combined) precision of our instruments (see Vogelmann et al., 2011).

The temporal variability of IWV can also be estimated from the standard deviation of differences of measurements recorded by the same instrument within certain time intervals. In our case, this was possible with data from the FTIR instrument only, thanks to its more frequent and continuous operation. The result is reflected by the blue curve in Fig. 5. Due to the solar FTIR's 13.3 min integration time, the curve starts at an interval length of Δt = 20 minutes. The blue curve begins to deviate increasingly from the green curve beyond 30 minutes and converges towards the red curve for larger time intervals. This corresponds to the fact that we observe a superposition of temporal and spatial variability with the solar FTIR, i.e., for larger time intervals, the FTIR instrument produces a spatial mismatch by itself: Due to its sun-pointing geometry, the FTIR instrument probes a different volume after a certain time. This spatial mismatch has a significant effect for time intervals longer than 30 minutes.

3 Profile Variability

The variability of the vertical water vapor distribution on time scales of Δt <= 5 h was derived from water vapor number density profiles retrieved from the DIAL measurements. We built ensembles of DIAL water vapor profiles recorded within a range of time intervals (e.g. 1 h - 5 h). After normalizing each profile by the respective ensemble mean profile, we merged all normalized profiles into a large ensemble for statistical analysis. First, we calculated the relative variance σ^2/μ^2 (with μ=ensemble mean number density) as a function of altitude for different time intervals. This is plotted on the left hand side of Fig. 6. For the shortest time interval of this investigation (1 h), the relative variance starts with a value of about 0.02. Above 5 km, the variance continuously increases to more than 0.38 at an altitude of about 11 km a.s.l.. For longer time intervals up to 5 hours, the relative variance behaves quite similarly, but is shifted to higher values at all altitudes. This is in agreement with our results of IWV variability analysis, according to which longer time intervals lead to larger variabilities at all altitudes. In comparison to the 1-h profile, we see a more significant maximum at the lower edge at 3 km and a significant minimum at 4.5 km for longer time intervals. .This enhanced increase between 3 km and 4 km is, to our understanding, induced by the diurnally varying upper edge of the boundary layer during the warm season (see below).

For the lowest layer (i.e. 3 - 4 km), where most of the entire column above ~~our~~ Zugspitze site is stored, we find equal relative variabilites as for IWV. This means that for a time interval Δt=1 h, the coefficient of variation σ/μ = 0.12. From the green curve in Fig. 5, we obtain a 1-h

variability of 0.27 mm with a 60-min ensemble mean IWV of 2.33 mm, which also yields a coefficient of variation of 0.12.

In contrast to this, the relative variability increases with altitude above 5 km. This can be explained by the increasing wind speed at higher altitudes in the troposphere. The temporal variability of the water vapor density in the free troposphere at a certain altitude primarily features a horizontal variability combined with a horizontal wind velocity at this altitude. From NCEP reanalysis data, we derived an average wind speed as a function of altitude, which increases from a few meters per second near the ground to about 22 m/s in the tropopause region (Fig. 7). Similar values were reported by Birner et al. (2002) based on radiosonde data recorded above Munich (South Germany). Depending on the pathway of the jet stream or the polar vortex, maximum wind velocities of more than 100 m/s occur occasionally (Riehl, 1962). Considering a time interval of 60 minutes, this means a mean horizontal spread of about 80 km around 10 km altitude with a potential increase to more than 360 km in the jet stream regime.

The general increase of the relative short-term variability of water vapor above 5 km (Fig. 6, left) seems to flatten slightly at about 10 km. This can be explained by the fact that the wind speed has its maximum here and decreases at higher altitudes. Above 9 km, the contribution of measurement errors becomes significant. The DIAL is not able to measure water vapor concentrations below 18 ppm (sensitivity limit at 10 km), which may be even lower in the tropopause region. Hence, for the calculation of variances and covariances, only profiles valid in the entire range (3 km – 12 km) are taken into account including a statistical error calculation.

The connectivity of the short-term variability of water vapor at different altitudes is analyzed using the covariance matrix of the vertical profile variability (Fig. 6, right). The covariance matrix is calculated from all normalized profiles recorded from 2007 to 2011, which are contained in the subensembles of profiles recorded within a 5-hour time interval. Consequently, the diagonal of the covariance matrix is identical to the 5-hour- curve of the variability profile shown on the left hand side of Fig. 6. There are no significant off-diagonal values below 6 km. We interpret this as a sign of the lower altitudes being not dominated by a coherent air flow for most of the observations. This means that the horizontal flow at certain altitudes below 6 km is not or only weakly coupled to the flow above or below. The slight increase of off-diagonal values between 6 km and 8 km indicates a partially coherent flow. The high off-diagonal values above 8 km indicate a large fraction of coherent flow of inhomogeneous air masses in this altitude region.

The weak coupling between different layers at lower altitudes is in agreement with the assumption of local convection and turbulence being the dominant sources of variability in the lower part of the examined altitude range. This behavior can be described by barely interacting ”bubbles” of humid air. In the upper troposphere, by contrast, varying air masses are more coherently exchanged within the upper air flow, as a result of which layers of a wider vertical spread are affected.

4 Mechanisms driving the variability ~~O~~observed

Evaporation is the only relevant source and precipitation the only relevant sink of water vapor in the troposphere. Thus, water vapor is injected into the free troposphere by uplifting processes, such as local convection or large-scale warm conveyor belts. These uplifting processes cause inhomogeneity in the horizontal water vapor distribution at a certain altitude. Furthermore, air ascending to high altitudes undergoes cooling. If this air initially was humid, part of its water vapor content can be precipitated during the ascent. As a result, the absolute humidity of upper tropospheric air is low in general. Downwelling of dry air from high altitudes, in particular from

the tropopause region or even the stratosphere, also produces inhomogeneity in the horizontal humidity field at the affected altitude levels. In contrast to uplifting processes, downwelling generally is not a local phenomenon. As regards the short-term variability (i.e. $\Delta t < 6$ h) of the vertical distribution of water vapor, it is reasonable to distinguish between inhomogeneity produced locally on a small scale and inhomogeneity produced remotely and transported on long-range pathways. By analyzing the measured water vapor profiles in combination with trajectory calculations from atmospheric models ~~HYSPLIT backward trajectories calculated from reanalysis data (http://ready.arl.noaa.gov/HYSPLIT.php, Draxler and Hess, 1998)~~, we found that the short-term variability of the profiles shows contributions from both local effects and long-range transport at the same time. The short-term variability above 5 km can be attributed to the advection of a heterogeneous layer structure in most cases. Below 5 km, by contrast, a clear assignment is not always possible. Backward trajectories were calculated from reanalysis data with the NOAA HYSPLIT vertical velocity model (http://ready.arl.noaa.gov/HYSPLIT.php, Draxler and Hess, 1998). However, the performance of a trajectory model is also limited above complex terrain and running times of several days occasionally involve large uncertainties even in the free troposphere. Sometimes several attempts are necessary to guess the correct start altitude due to shifts in the orographic data used by the model (Trickl et al., 2010). Thus, trajectory calculations are not considered as a proof, but as suggestion for plausibility. In our trajectory analyses for atmospheric long-range transport over many years, we have seen a good reliability within the free troposphere in most cases.~~.~~ In the following subsections we highlight four different types of dynamics producing short-term variability of water vapor.

4.1. Local convection

4.1.1 Case studies

A case of local convection under stable atmospheric conditions (high pressure) is shown in Fig. 8. Three water vapor profiles were recorded within 40 minutes. The variability stops at the upper edge of the boundary layer at 3.5 km. Above this level, the water vapor distribution remains constant throughout that period. The upper edge of the boundary layer was visually verified by the upper edge of cumulus clouds located at the top of some thermals. Strongly enhanced backscatter from boundary layer aerosols is recorded up to 3.5 km. Some weaker aerosol structure that slowly moves downwards is observed above 4.5 km and even up to 7.1 km.

The situation is somewhat different under low pressure and atmospheric instability. This case is shown in Fig. 9. Five profiles were recorded within a time interval of 4 h before a heavy thunderstorm developed in the afternoon. The short-term variability of water vapor is rather high and reaches far into the upper troposphere up to at least 7.5 km. Due to the travel time of upwelling air and the increasing horizontal wind speed, the variations at high altitudes (e.g. above 5 km) are less local than the variations near the ground. Cloud formation is first observed between 5.5 km and 6.5 km. But only a few minutes later, clouds form also above 2.5 km. Due to cloud interference, the last valid profile was recorded at 11:10 UTC (local time - 1 h). Strongly enhanced backscatter from boundary-layer aerosols was recorded up to 4.7 km in the morning already (7:03 UTC). This altitude is rather high. The latest profile at 11:10 UTC exhibits boundary-layer aerosols up to 4.2 km only and also a lower humidity compared to the profiles recorded before. To our understanding, this indicates a downflow near, but outside of the thunderstorm. This downwelling air probably lost most of its original water content during its ascent in the thunderstorm by precipitation. At 12:37 UTC (profile not shown), the extended head of the cumulonimbus cloud of the upcoming thunderstorm overcasts the site above 7.7 km already. In addition, strong aerosol structures appear up to 7.5 km. Backward trajectory

calculations (HYSPLIT) suggest that air between 6 km and 7.5 km originated from the Caribbean boundary layer.

4.1.2 General discussion

During the warm season, local convection ~~and "Alpine pumping"~~ usually reaches altitudes of up to 1.5 km above summit levels (Carnuth and Trickl, 2000; Carnuth et al., 2002; Kreipl, 2005), which is about 4.5 km a.s.l. in our case. The enhanced updraft along sunny mountain slopes is nicknamed "Alpine pumping". The slightly elevated short-term variability at lower altitudes around 3.5 km (Fig. 6, left) is attributed to local convection and the diurnal variation of the upper edge of the planetary boundary layer, which is caused by Alpine pumping. Due to the strong vertical gradient of the water vapor profile, this dominates the short-term variability of IWV in most cases when local convection significantly exceeds 3 km (which is the bottom of our measurement range). From the comparatively low mean wind speed at lower altitudes (Fig. 7), we conclude that the elevated variability here is caused by larger horizontal gradients in the water vapor concentration. This means that variations occur on smaller horizontal scales compared to higher altitudes, which underlines that local processes on small scales are the dominant source, e.g. thermal lifts. Short-term variations of the water vapor concentration at a certain altitude within the upper part of the boundary layer (i.e. 3 km – 4.5 km a.s.l.), which are caused by local convection, are estimated to be smaller than a factor of 2. Convection ~~intruding~~ penetrating into the free troposphere or even the upper troposphere can cause short-term variation factors of more than 5 at these high altitudes (e.g. Fig. 9, other observations). The presence of aerosols (enhanced backscatter) usually indicates upwelling air from the planetary boundary layer. Aerosol structures in the free troposphere are also helpful for estimating the vertical velocity of the probed air. Both cases were visually verified by the observation of cloud formation, while trajectory calculations from models are not able to resolve these small-scale local processes. But, they indicate a general downwelling for the case under stable high pressure conditions and a general upwelling for the case under unstable low pressure conditions.

4.2. Long-range transport

4.2.1 Case studies

Figures 10 and 11 show cases of extreme vertical variability of water vapor on a time scale of hours recorded with the DIAL. Similar scenarios have been observed many times. From these incidents we learned that the water-vapor density at a certain altitude can vary by a factor of more than 30 within a few hours. Thus, the short-term variability of water vapor induced by long-range transport and the advection of very inhomogeneous layer structures can exceed the impact of local convection by one order of magnitude.

This is particularly pronounced for stratospheric intrusions that descend from the Arctic to Central Europe. These intrusion layers can occasionally become the main source of short-term variability of water vapor in the altitude range between 3 km and 5 km. However, such events occur predominantly during the winter season and are accompanied with non convective weather conditions. ~~Stratospheric intrusions into the lower free troposphere usually occur in the winter season with a frequency of roughly 4 to 10 times per month above our site (Stohl et al., 2000; Trickl et al., 2010).~~Under these~~is~~ conditions heterogeneous air masses are usually advected with a high velocity which results in a very high variability at certain altitudes even on the short timescale of one hour. Due to the origin of these layers, stratospheric intrusion events are usually

accompanied by rather dry conditions. This is illustrated by the example given in Fig. 10 where three layers of stratospheric air have been advected at the same time at different altitudes, thus, creating relative variations of the water vapor density of more than a factor of 10 at certain altitudes within 4 hours. Forward trajectory calculations with the Lagrangian model "LAGRANTO" by ETH Zürich (Wernli and Davies, 1997) illustrate the very complex dynamics and its accompanying heterogeneous vertical layering (Fig. 11). Several pathways originating in the Arctic stratosphere hit the location of Mt. Zugspitze at different altitudes about the same time on March 6, 2008. This ~~very complex~~ case, including the trajectory calculation, is discussed in more detail in a separate publication (Trickl et al., 2014 and references therein.). Stratospheric intrusions into the lower free troposphere usually occur in the winter season with a frequency of roughly 4 to 10 times per month above Mt. Zugspitze (Stohl et al., 2000; Trickl et al., 2010).

Also humid air from remote boundary layers sometimes causes rather intense short-term variations of the water vapor distribution. An example is shown in Fig. 12~~1~~. The humidity profile suffers a significant increase between 4 and 5 km a.s.l. within two hours. Backward trajectory calculations from reanalysis data with the HYSPLIT vertical velocity model (see above)~~(from reanalysis data)~~ for this case ~~indicate that the origin of the advected air at an altitude of 4.7 km a.s.l. changes from the subarctic upper troposphere (dry) to the Pacific boundary layer (rather humid) within two hours~~ suggest a sudden change in the source region from the North American upper troposphere (dry) to the North-West Pacific boundary layer (rather humid) within two hours (Fig. 11).~~,~~ ~~while the~~ In contrast, air at an altitude of about 3.3 km constantly originates from the subtropical North Atlantic boundary layer (moderately humid, trajectories not shown here). The trajector~~y~~ies starting in the North-West Pacific boundary layer exhibits a fast ascent to the UT within 2 days. This behavior is attributed to a warm conveyor belt using the criteria published by Eckhardt et al. (2004). Satellite images show that the ascending part of the trajectory is near the warm front of a cyclone that is located about 2000 km south of the peninsula of Kamchatka (North-West Pacific Ocean). Warm conveyor belts are known to be the most important extra-tropical transport mechanism of water vapor to the free and upper troposphere, although the water vapor flux moves like a jet from a rather restricted area (Browning and Roberts, 1994; Browning et al., 1997; Eckhardt et al., 2004; Ziv et al., 2009). It is remarkable that these filamentary structures are partially preserved, while traveling around half the hemisphere. A wind speed of 16 m/s at an altitude of 4.5 km (Munich radiosonde, 12 UTC) transforms a time shift of two hours into a horizontal shift of about 115 km. The water vapor density at this altitude changes by more than a factor of 5 within 2 hours in this case.

4.2.2 General discussion

It is reasonable to assume that much of the variability in the free troposphere is caused by the rich layer structure advected along or in the vicinity of the North Atlantic storm track or from the Mediterranean basin and North Africa. From our lidar measurements of ozone, water vapor, and aerosol, we know that the persistence of specific free tropospheric layers above ~~our site~~Mt. Zugspitze can range from less than one hour to more than one day (Eisele et al., 1999; Stohl and Trickl, 1999; Trickl et al., 2003, 2010, 2011;). Along the jet stream, a lot of different ascending and descending air streams merge or separate (e.g. Appenzeller et al., 1996; Stohl et al., 2001; Cooper et al., 2001, 2002, 2004a, 2004b; Flentje et al., 2005). The advection of filamentary and heterogeneous layer structures affects the entire free troposphere and dominates the variability of water vapor in the upper troposphere above 5 km. The most important source regions contributing to observations above ~~our site~~ Mt. Zugspitze have been the stratosphere (very dry air), North America, the (sub)tropical Atlantic (very humid), but also Asia. Sometimes, dry and ozone-rich air flows along the northward spiraling subtropical jet streams (Trickl et al., 2011). The layers

frequently possess a meridional component, leading to a transverse passage of adjacent layers across the observational site. This implies a rapid change in concentrations.

5. Summary and conclusions

The result of our studies is a quantitative description of the short-term variability of water vapor in the free troposphere above Mt. Zugspitze, which is a location representative of Central Europe. From measurement data recorded with two high-precision optical water vapor sounders arranged in a unique pointing geometry, we derived information about the spatio-temporal variability of integrated water vapor (IWV) on the 1 km-scale and on the minutes scale.

Within a time interval of 20 minutes, a variability of about 0.35 mm was determined in the summer season under the condition of good volume matching ($\Delta x < 2$ km). The spatial variability became significant for horizontal distances above 2 km, but only in the warm season. The variability of IWV observed in the winter season ~~generally~~ was generally lower and did not increase with a horizontal mismatch of the probed volume ($\Delta x < 12$ km). Its absolute value, however, was larger than in the summer season. The seasonality of the IWV short-term variability and the geometrical restrictions of the measurements underline that local convection is the main source of variability ~~in~~ during the ~~summer~~ warm season, while the variability in the winter season is driven by dynamics on a larger scale. The temporal variability of IWV was determined to be 0.05 mm on the minute scale (5 min) with a uniform increase to 0.5 mm on the time scale of one day.

The free tropospheric profile variability of water vapor on the time scale of hours (e.g., 1 h—5 h) shows a broad minimum around 4.5 km a.s.l. and much larger values for higher altitudes with a constant increase up to the tropopause region. Longer time intervals generally yield larger variations at all altitudes and additionally show a more significant maximum at the lower edge of the measurement range (3 km). These findings are explained by the vertical wind profile and the heterogeneity of air masses within the upper air flow advected with a high velocity and, additionally, by the impact of local convection below 4.5 km. The covariance matrix of the profile variability yields information about the connectivity of neighboring layers and shows that the air flow below 6 km is rather incoherent, while the upper air stream above 8 km is much more coherent.

We presented four~~4~~ case studies in which the profile variability of water vapor on the time scale of hours was attributed to specific mechanisms: Local and vertically limited convection under stable conditions, high-reaching convection under unstable conditions, downwelling of a stratospheric intrusion, and long-range transport from very different source regions.

The source of the variability can be either local convection or long-range transport of inhomogeneous air masses. When reviewing all profiles of our study, we found that it is not always possible to distinguish clearly between both mechanisms of short-term variability. In particular, for altitudes below 4.5 km, which are potentially affected by local convection even under stable atmospheric conditions, we ~~have to~~ must assume a mixture of both local contributions and the advection of inhomogeneous layer structures from different remote source regions. From cases where a clear assignment was possible, we conclude that the long-range advection of very inhomogeneous layer structures can cause relative~~ly~~ short-term variations of the water vapor concentration at a certain altitude, which are larger by one order of magnitude than variations in cases dominated by the impact of local convection. Due to the high altitude of the measurement site, our analysis is mostly restricted to the free troposphere. The upper edge of the Alpine boundary layer reaches our measurement range usually only during afternoons in the

summer season. It is a consequence of measuring above a complex alpine terrain (steep mountain slopes) that we observe the influence of local convection in our measurement range (above 3 km a.s.l.) quite frequently. The impact of local convection undercuts the possible impact of long range-transport by roughly one order of magnitude. This suggests, at least for the summer season, that the variability inside the boundary layer is probably reduced to values that we observe with dominating local convection reaching our measurement range. This assumption, of course, implies that the fast advection of heterogeneous air layers does not impact the boundary layer.

In spite of the missing convection, the relative~~ly~~ short-term variability of water vapor (IWV and profiles) in the free troposphere is higher during the winter season. This is explained by the results of Trickl (2010), according to which ~~most~~ stratospheric air intrusions above Mt. Zugspitze exhibit a pronounced maximum ~~pass Mt. Zugspitze between 2 km and 4 km a.s.l., primarily~~ during the winter season. Roughly 3/4 of them reach the Zugspitze summit (2962 m) and were detected directly by the in-situ instrumentation.

Our results for the first time provide ~~for~~ a quantitative description of the free tropospheric spatio-temporal variability of water vapor on the scales of minutes and kilometers (horizontal) for IWV and the scales of hours and 500 m (vertical) for profiles. This information can be useful for the parameterization of humidity in atmospheric models as well as for estimating the influence of the atmospheric variability of water vapor on the significance of water vapor measurements performed with a given integration time. In a related sense our results also provide the information necessary for evaluating intercomparison studies of not perfectly co-located or synchronized instruments. Our findings fit perfectly to the results of our previous intercomparison study (Vogelmann et al., 2011) that already indicated a high variability of water vapor, as a result of which very tight matching criteria are required down to the scales of 10 minutes and several hundred meters to reduce co-location-effects to a negligible level. -

Acknowledgements. We thank Hans-Peter Schmid (KIT/IMK-IFU) for his continuous interest in this work and M. Rettinger (KIT/IMK-IFU) for executing the FITR measurements at Mt. Zugspitze. We also thank Michael Sprenger (ETH Zürich) for providing the forward trajectory calculations (for the analysis of stratosphere to troposphere transport). We also acknowledge the team of the Schneefernerhaus research station (UFS) for maintaining our lidar measurements and the Bavarian Ministry of Environment and Consumer Protection for funding our work within the ALOMAR cooperation.

References

Adam, M., Demoz, B. B., Whiteman, D. N., Venable, D. D., Joseph, E., Gambacorta, A., Wei, J., Shephard, M. W., Miloshevich, L. M., Barnet, C. D., Herman, R. L., Fitzgibbon, J., and Connell, R.: Water Vapor Measurements by Howard University Raman Lidar during the WAVES 2006 Campaign, J. Atmos. Ocean. Tech., 27, 42, doi: 10.1175/2009JTECHA1331.1, 2010.

Appenzeller, C., Davies, H. C., and Norton, W. A.: Fragmentation of stratospheric intrusions, J. Geophys. Res., 101, 1435—1456, 1996.

Birner, T., Dörnbrack, A., and Schumann, U.: How sharp is the tropopause at midlatitudes? , Geophys. Rev. Lett., 29, 1700, doi: 10.1029/2002GL015142, 2002.

Bleisch, R., Kämpfer, N., and Haefele, A.: Retrieval of tropospheric water vapour by using spectra of a 22 GHz radiometer, Atmos. Meas. Tech., 4, 1891–1903, doi: 10.5194/amt-4-1891-2011, 2011.

Browning, K. A. and Roberts, N. M.: Structure of a frontal cyclone, Quarterly Journal of the Royal Meteorological Society, 120, 1535–1557, doi: 10.1002/qj.49712052006, 1994.

Browning, K. A., Roberts, N. M., and Illingworth, A. J.: Mesoscale analysis of the activation of a cold front during cyclogenesis, Quarterly Journal of the Royal Meteorological Society, 123, 2349–2375, doi: 10.1002/qj.49712354410, 1997.

Carnuth, W. and Trickl, T.: Transport studies with the IFU three-wavelength aerosol lidar during the VOTALP Mesolcina experiment, Atmos. Environ., 34, 1425–1434, 2000.

Carnuth, W., Kempfer, U., and Trickl, T.: Highlights of the tropospheric lidar studies at IFU within the TOR project, Tellus, 54B, 163–185, 2002.

Cooper, O., Forster, C., Parrish, D., Dunlea, E., Hübler, G., Fehsenfeld, F., Holloway, J., Oltmans, S., Johnson, B., Wimmers, A., and Horowitz, L.: On the life cycle of a stratospheric intrusion and its dispersion into polluted warm conveyor belts, J. Geophys. Res., 109, D23S09, doi: 10.1029/2003JD004006, 2004a.

Cooper, O. R., Moody, J. L., Parrish, D. D., Trainer, M., Ryerson, T. B., Holloway, J. S., Hübler, G., Fehsenfeld, F. C., Oltmans, S. J., and Evans, M. J.: Trace gas signatures of the airstreams within North Atlantic cyclones: Case studies from the North Atlantic Regional Experiment (NARE 97), J. Geophys. Res., 106, 5437–5456, doi: 10.1029/2000JD900574, 2001.

Cooper, O. R., Moody, J. L., Parrish, D. D., Trainer, M., Holloway, J. S., Hübler, G., Fehsenfeld, F. C., and Stohl, A.: Trace gas composition of midlatitude cyclones over the western North Atlantic Ocean: A seasonal comparison of O_3 and CO, J. Geophys. Res., 107, 4057, doi: 10.1029/2001JD000902, 2002.

Cooper, O. R., Forster, C., Parrish, D., Trainer, M., Dunlea, E., Ryerson, T., Hübler, G., Fehsenfeld, F., Nicks, D., Holloway, J., de Gouw, J., Warneke, C., Roberts, J. M., Flocke, F., and Moody, J.: A case study of transpacific warm conveyor belt transport: Influence of merging airstreams on trace gas import to North America, J. Geophys. Res., 109, D23S08, doi: 10.1029/2003JD003624, 2004b.

Draxler, R. R. and Hess, G. D.: An Overview of the HYSPLIT_4 Modelling System for Trajectories, Dispersion, and Deposition, Australian Meteorological Magazine, 47, 295–308, 1998.

Eckhardt, S., Stohl, A., Wernli, H., James, P., Forster, C., and Spichtinger, N.: A 15-Year Climatology of Warm Conveyor Belts, Journal of Climate, 17, 218–237, doi: 10.1175/1520-0442(2004)017<0218:AYCOWC>2.0.CO;2, 2004.

Eisele, H., Scheel, H. E., Sládkovič, R., and Trickl, T.: High-Resolution Lidar Measurements of Stratosphere-Troposphere Exchange, J. Atmos. Sci., 56, 319–330, 1999.

Fassò, A., Ignaccolo, R., Madonna, F., Demoz, B. B., and Franco-Villoria, M.: Statistical modelling of collocation uncertainty in atmospheric thermodynamic profiles, Atmos. Meas. Tech., 7, doi: 1803-1816, 10.5194/amt-7-1803-2014, 2014.

Flentje, H., Dörnbrack, A., Ehret, G., Fix, A., Kiemle, C., Poberaj, G., and Wirth, M.: Water vapor heterogeneity related to tropopause folds over the North Atlantic revealed by airborne water vapor differential absorption lidar, J. Geophys. Res., 110, D03115, doi:10.1029/2004JD004957, 2005.

Harries, J. E.: Atmospheric radiation and atmospheric humidity, Q. J. R. Meteor. Soc., 123, 2173–2186, 1997.

Immler, F. J., Dykema, J., Gardiner, T., Whiteman, D. N., Thorne, P. W., and Vömel, H.: Reference Quality Upper-Air Measurements: guidance for developing GRUAN data products, Atmos. Meas. Tech., 3, 1217–1231, doi: 10.5194/amt-3-1217-2010, 2010.

Kiehl, J. T. and Trenberth, K. E.: Earth's Annual Global Mean Energy Budget, B. Am. Meteorol. Soc., 78, 197–208, 1997.

Kreipl, S.: Messung des Aerosoltransports am Alpennordrand mittels Laserradar (Lidar), Dissertation (in German), Universität Erlangen, 2006.

Kämpfer, N., ed.: Monitoring Atmospheric Water Vapour - Ground-Based Remote Sensing and In-situ Methods, Springer, Berlin, Heidelberg, 2013.

Leblanc, T., Walsh, T. D., McDermid, I. S., Toon, G. C., Blavier, J.-F., Haines, B., Read, W. G., Herman, B., Fetzer, E., Sander, S., Pongetti, T., Whiteman, D. N., McGee, T. G., Twigg, L., Sumnicht, G., Venable, D., Calhoun, M., Dirisu, A., Hurst, D., Jordan, A., Hall, E., Miloshevich, L., Vömel, H., Straub, C., Kampfer, N., Nedoluha, G. E., Gomez, R. M., Holub, K., Gutman, S., Braun, J., Vanhove, T., Stiller, G., and Hauchecorne, A.: Measurements of Humidity in the Atmosphere and Validation Experiments (MOHAVE)-2009: overview of campaign operations and results, Atmos. Meas. Tech., 4, 2579–2605, doi: 10.5194/amt-4-2579-2011, 2011.

Müller, H. and Reiter, R.: Untersuchung der Gebirgsgrenzschicht über einem großen Alpental bei Berg-Talwindzirkulation, Meteorol. Rdsch., 39, 247–256 (in German), 1986.

Pougatchev, N. S., Connor, B. J., and Rinsland, C. P.: Infrared measurements of the ozone vertical distribution above Kitt Peak, J. Geophys. Res., 100, 16 689–16 697, doi: 10.1029/95JD01296, 1995.

Reiter, R., Müller, H., Sladkovic, R., and Munzert, K.: Aerologische Untersuchungen der tagesperiodischen Gebirgswinde unter besonderer Berücksichtigung des Windfeldes im Talquerschnitt, Meteorol. Rdsch., 36, 225–242 (in German), 1983.

Riehl, H.: Jet Streams of the Atmosphere, Tech. Rep. 32, Department of Atmospheric Science Colorado State University Fort Collins, Colorado, 1962.

Seidel, D. J., Sun, B., Pettey, M., and Reale, A.: Global radiosonde balloon drift statistics, J. Geophys. Res., 116, D07102, doi: 10.1029/2010JD014891, 2011.

Soden, B. J. and Lanzante, J. R.: An Assessment of Satellite and Radiosonde Climatologies of Upper-Tropospheric Water Vapor., J. Clim., 9, 1235–1250, doi: 10.1175/1520-0442(1996)009<1235:AAOSAR>2.0.CO;2, 1996.

Stiller, G. P., Kiefer, M., Eckert, E., von Clarmann, T., Kellmann, S., García-Comas, M., Funke, B., Leblanc, T., Fetzer, E., Froidevaux, L., Gomez, M., Hall, E., Hurst, D., Jordan, A., Kämpfer, N., Lambert, A., McDermid, I. S., McGee, T., Miloshevich, L., Nedoluha, G., Read, W., Schneider, M., Schwartz, M., Straub, C., Toon, G., Twigg, L. W., Walker, K., and Whiteman, D. N.: Validation of MIPAS IMK/IAA temperature, water vapor, and ozone profiles with MOHAVE-2009 campaign measurements, Atmos. Meas. Tech., 5, 289–320, doi: 10.5194/amt-5-289-2012, 2012.

Stohl, A.: A 1-year Lagrangian “climatology” of airstreams in the Northern Hemisphere troposphere and lowermost stratosphere, J. Geophys. Res., 106, 7263–7280, doi: 10.1029/2000JD900570, 2001.

Stohl, A. and Trickl, T.: A textbook example of long-range transport: Simultaneous observation of ozone maxima of stratospheric and North American origin in the free troposphere over Europe, J. Geophys. Res., 104, 30 445–30 462, doi: 10.1029/1999JD900803, 1999.

Stohl, A., Spichtinger-Rakowsky, N., Bonasoni, P., Feldmann, H., Memmesheimer, M., Scheel, H. E., Trickl, T., Hübener, S., Ringer, W., and Mandl, M.: The influence of stratospheric intrusions on alpine ozone concentrations, Atmos. Env., 34, 1323–1354, doi: 10.1016/S1352-2310(99)00320-9, 2000.

Sun, B., Reale, A., Seidel, D. J., and Hunt, D. C.: Comparing radiosonde and COSMIC atmospheric profile data to quantify differences among radiosonde types and the effects of imperfect collocation on comparison statistics, J. Geophys. Res., 115, D23104, doi: 10.1029/2010JD014457, 2010.

Sussmann, R. and Schäfer, K.: Infrared spectroscopy of tropospheric trace gases: combined analysis of horizontal and vertical column abundances, Appl. Opt., 36, 735–741, doi: 10.1364/AO.36.000735, 1997.

Sussmann, R., Borsdorff, T., Rettinger, M., Camy-Peyret, C., Demoulin, P., Duchatelet, P., Mahieu, E., and Servais, C.: Technical Note: Harmonized retrieval of column-integrated atmospheric water vapor from the FTIR network – first examples for long-term records and station trends, Atmos. Chem. Phys., 9, 8987–8999, doi: 10.5194/acp-9-8987-2009, URL http://www.atmos-chem-phys.net/9/8987/2009/, 2009.

Tobin, D. C., Revercomb, H. E., Knuteson, R. O., Lesht, B. M., Strow, L. L., Hannon, S. E., Feltz, W. F., Moy, L. A., Fetzer, E. J., and Cress, T. S.: Atmospheric Radiation Measurement site atmospheric state best estimates for Atmospheric Infrared Sounder temperature and water vapor retrieval validation, J. Geophys. Res., 111, D09S14, doi: 10.1029/2005JD006103, 2006.

Trenberth, K.: Atmospheric Moisture Residence Times and Cycling: Implications for Rainfall Rates and Climate Change, Clim. Change, 39, 667-694, doi: 10.1023/A:1005319109110, 1998.

Trenberth, K., Jones, P., Ambenje, P., Bojariu, R., Easterling, D., Tank, A., Parker, D., Rahimzadeh, F., Renwick, J., Rusticucci, M., Soden, B., and Zhai, P.: Observations: Surface and Atmospheric Climate Change. In Climate Change 2007: The Physical Science Basis. Contribution of Working Group I to the Fourth Assessment Report of the Intergovernmental Panel on Climate Change, chap. 3, pp. 235–336, Cambridge, United Kingdom and New York, N.Y., USA: Cambridge University Press, 2007.

Trickl, T., Cooper, O. R., Eisele, H., James, P., Mücke, R., and Stohl, A.: Intercontinental transport and its influence on the ozone concentrations over central Europe: Three case studies, J. Geophys. Res., 108, 8530, doi: 10.1029/2002JD002735, 2003.

Trickl, T., Feldmann, H., Kanter, H.-J., Scheel, H.-E., Sprenger, M., Stohl, A., and Wernli, H.: Forecasted deep stratospheric intrusions over Central Europe: case studies and climatologies, Atmos. Chem. Phys., 10, 499–524, doi: 10.5194/acp-10-499-2010, URL http://www.atmos-chem-phys.net/10/499/2010/, 2010.

Trickl, T., Eisele, H., Bärtsch-Ritter, N., Furger, M., Mücke, R., Sprenger, M., and Stohl, A.: High-ozone layers in the middle and upper troposphere above Central Europe: potential import from the stratosphere along the subtropical jet stream, Atmos. Chem. Phys, 11, 9343–9366, 2011.

Trickl, T., Vogelmann, H., Giehl, H., Scheel, H.-E., Sprenger, M., and Stohl, A.: How stratospheric are deep stratospheric intrusions?, Atmos. Chem. Phys., 14, 9941–9961, doi: 10.5194/acp-14-9941-2014, URL http://www.atmos-chem-phys.net/14/9941/2014/, 2014.

Turner, D. D. and Mlawer, E. J.: The Radiative Heating in Underexplored Bands Campaigns, Bulletin of the American Meteorological Society, 91, 911–923, doi: 10.1175/2010BAMS2904.1, 2010.

VDI guideline 4210: Remote sensing, Atmospheric measurements with LIDAR, Measuring gaseous air pollution with the LIDAR, Verein Deutscher Ingenieure, Beuth Verlag, Berlin, 47 pp., 1999.

Vogelmann, H. and Trickl, T.: Wide Range Sounding of Free Tropospheric Water Vapor with a Differential Absorption Lidar (DIAL) at a High Altitude Station, Appl. Opt., 47, 2116–2132, 10.1364/AO.47.002116, 2008.

Vogelmann, H., Sussmann, R., Trickl, T., and Borsdorff, T.: Intercomparison of atmospheric water vapor soundings from the differential absorption lidar (DIAL) and the solar FTIR system on Mt. Zugspitze, Atmos. Meas. Tech., 4, 835–841, doi: 10.5194/amt-4-835-2011, URL http://www.atmos-meas-tech.net/4/835/2011/, 2011.

Wagner, T., Beirle, S., Grzegorski, M., and Platt, U.: Global trends (1996-2003) of total column precipitable water observed by Global Ozone Monitoring Experiment (GOME) on ERS-2 and their relation to near-surface temperature, J. Geophys. Res., 111, D12102, doi: 10.1029/2005JD006523, 2006.

Wernli, H. and Davies, H. C.: A Lagrangian-based analysis of ex tratropical cyclones. I. The method and some applications, Q. J. Roy. Meteor. Soc., 123, 467–489, 1997.

Whiteman, D. N., Russo, F., Demoz, B., Miloshevich, L. M., Veselovskii, I., Hannon, S., Wang, Z., Vömel, H., Schmidlin, F., Lesht, B., Moore, P. J., Beebe, A. S., Gambacorta, A., and Barnet, C.: Analysis of Raman lidar and radiosonde measurements from the AWEX-G field campaign and its relation to Aqua validation, J. Geophys. Res., 111, D09S09, doi: 10.1029/2005JD006429, 2006.

Wirth, M., Fix, A., Ehret, G., Reichardt, J., Begie, R., Engelbart, D., Vömel, H., Calpini, B., Romanens, G., Apituley, A., Wilson, K. M., Vogelmann, H., and Trickl, T.: Intercomparison of Airborne Water Vapour DIAL Measurements with Ground Based Remote Sensing and Radiosondes within the Framework of LUAMI 2008, in: Proceedings of the 8th International Symposium on Tropospheric Profiling, edited by Apituley, A., Russchenberg, H., and Monna, W., Delft, The Netherlands, poster presentation, 2009.

Ziv, B., Saaroni, H., Romem, M., Heifetz, E., Harnik, N., and Baharad, A.: Analysis of conveyor belts in winter Mediterranean cyclones, Theor. Appl. Climatol., p. 124, doi: 10.1007/s00704-009-0150-9, 2009.

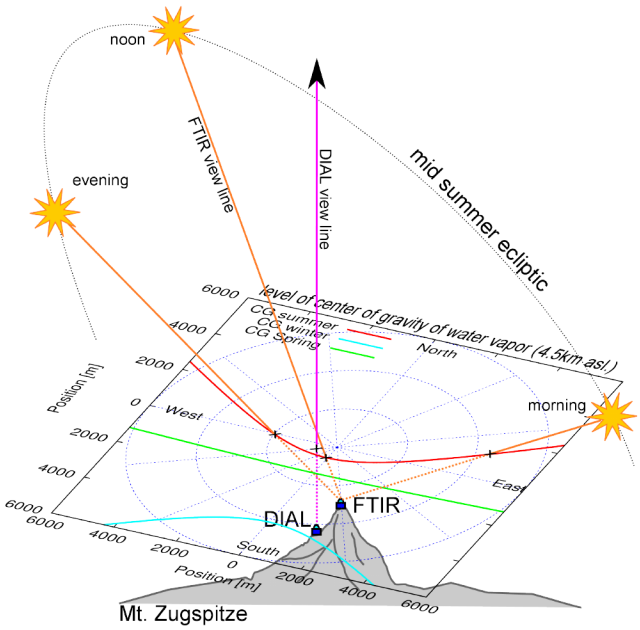

Figure 1: Geometrical setup of the IWV intercomparison between DIAL and FTIR on Mt. Zugspitze. The DIAL is located 680 m to the south-west of the FTIR and 288 m below. The horizontal coordinate grid plane (CG-plane) marks the mean altitude of the center of gravity of the water vapor distribution above MT. Zugspitze (see text) and has its point of origin vertical above the FTIR. The red, green, and blue curves in the CG-plane are the trajectories of the points, where the view line (e.g., orange lines from FTIR to the sun in the case of midsummer) of the FTIR meets the CG-plane in midsummer, spring, and midwinter. Consequently, the trajectories mark the horizontal positions of the center of gravity of the ~~vertical~~ water vapor distribution measured by the FTIR along its slanted view line. The pink line marks the fixed vertical view~~ing~~ line of the DIAL.

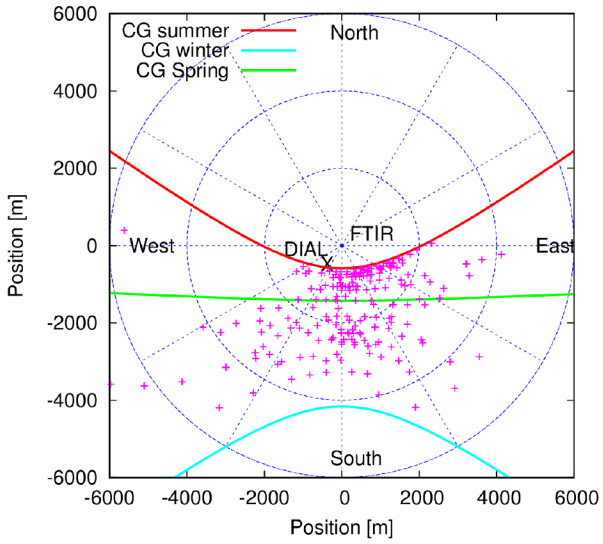

Figure 2: Trajectories of the horizontal positions of the center of gravity (CG) of the vertical water vapor distribution measured by the FTIR for IWV in midsummer, spring, and midwinter. Center of gravity horizontal locations from FTIR measurements coinciding with DIAL measurements ($\Delta t \leq 30$ min) are marked by crosses.

20

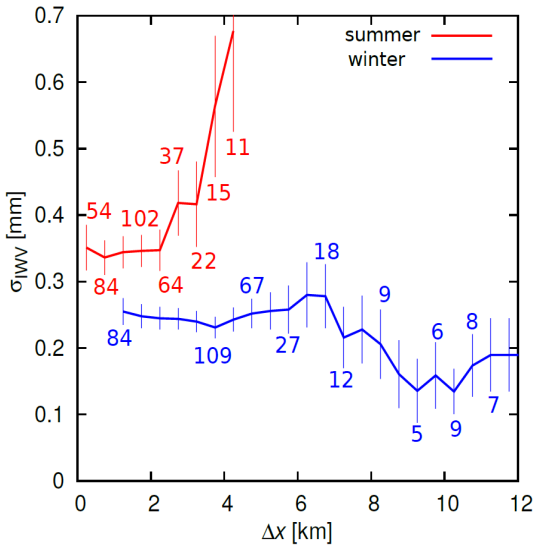

Figure 3: σ_{IWV} as a function of the horizontal distance Δx between the center of gravity of FTIR IWV and DIAL IWV in the summer season (red) and in the winter season (blue). The coincidence time interval Δt is 60 min for the blue curve and 30 min for the red ~~both~~ curve~~s~~ ~~(Δt = 60 min)~~. For geometrical reasons, the shortest distance in the winter season is 1 km. The ~~quantity~~ number of measurement pairs from which σ_{IWV} was calculated is indicated by the numbers near the curves (not for all nodes). The uncertainties (+- σ) are indicated by the error bars (for calculation see text).

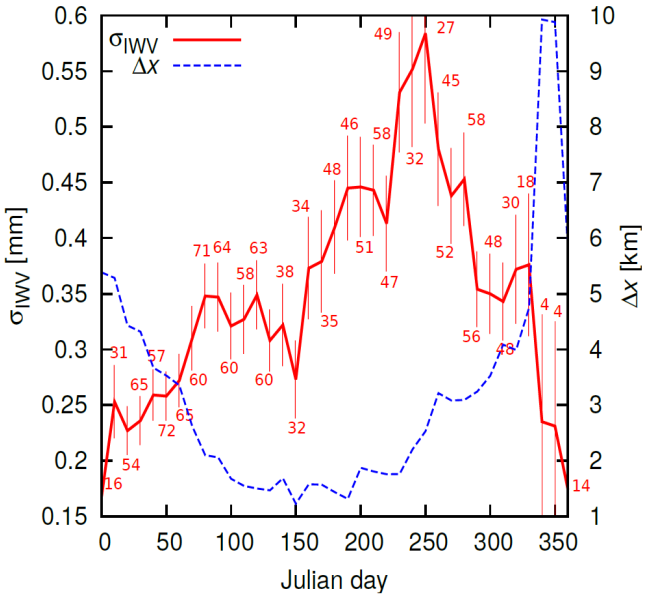

Figure 4: σ_{IWV} as a function of Julian day. The coincidence interval is 20 minutes in this case, pairs within 30 days were taken into account. The quantity of measurement pairs from which σ_{IWV} was calculated is indicated by the numbers near the curve. The dashed line shows the mean horizontal distance between the pairwise soundings of IWV as a function of the season. The uncertainties (+- σ) are indicated by the errorbars (for calculation see text).

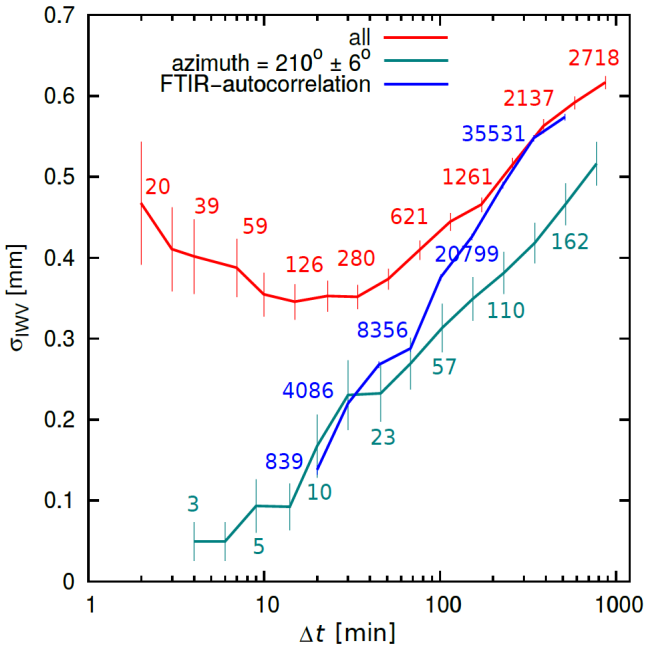

Figure 5: Variability as a function of the length of the time interval. The red curve shows σ_{IWV} from all measurements with no geometrical restrictions as a function of the length of the time interval in which data were taken into account. The green curve only includes measurements recorded in the early afternoon when the volume matching peaks with a sun azimuth of 210° ± 6°. The blue curve only shows σ_{IWV} of IWV values from the FTIR instrument. The quantity of measurement pairs from which σ_{IWV} was calculated is indicated by the numbers near the curves (not for all nodes). The uncertainties (+- σ) are indicated by the errorbars (for calculation see text).

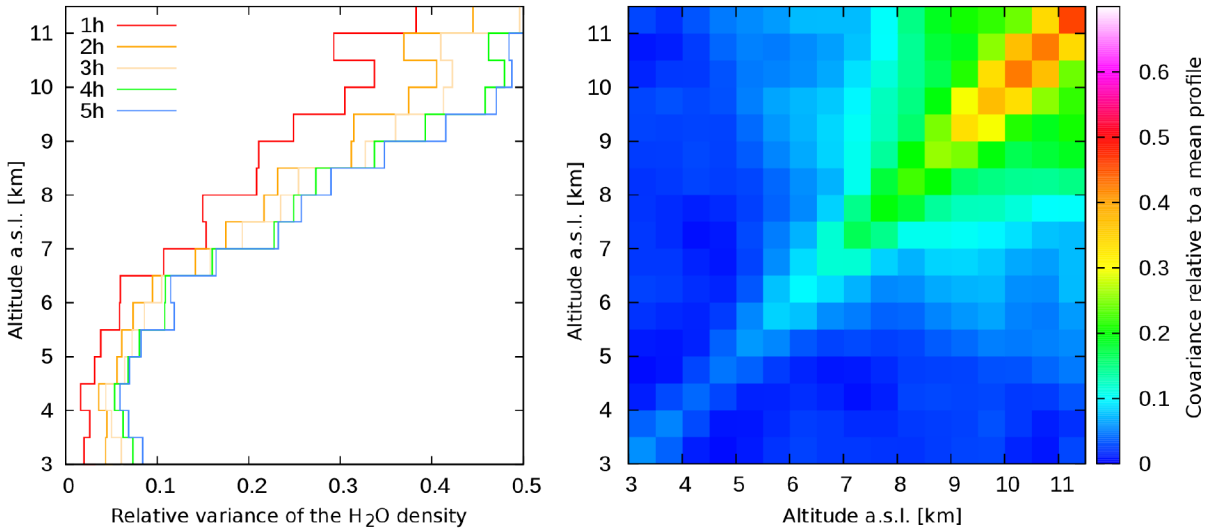

Figure 6: The short-term variability of the vertical water vapor profile is illustrated by the plot of the relative variance as a function of altitude within different time intervals (left plot). The covariance matrix (right plot) gives an idea of the interconnectivity of the variation between different altitudes.

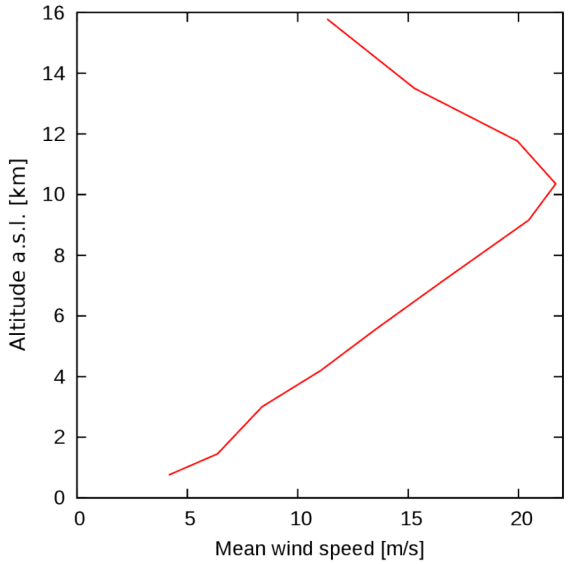

Figure 7: Mean wind speed above Mt. Zugspitze as a function of altitude (data from the National Center for Environmental Prediction, NCEP). Under the regime of the jet stream, the wind velocity at 10 km can occasionally exceed 100 m/s.

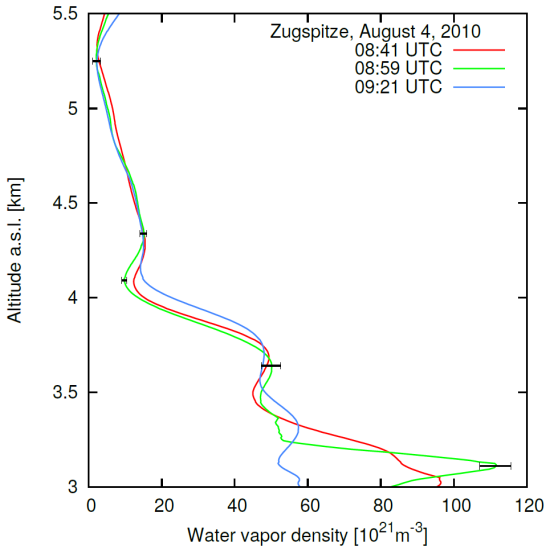

Figure 8: Short-term variability of the water vapor profile induced by local convection within a clearly confined upper edge of the boundary layer at 3.5. km under stable atmospheric conditions. The variations do not exceed a factor of 2. The example error bars (+- 2σ) represent statistical uncertainties caused by electronic noise in the detection.

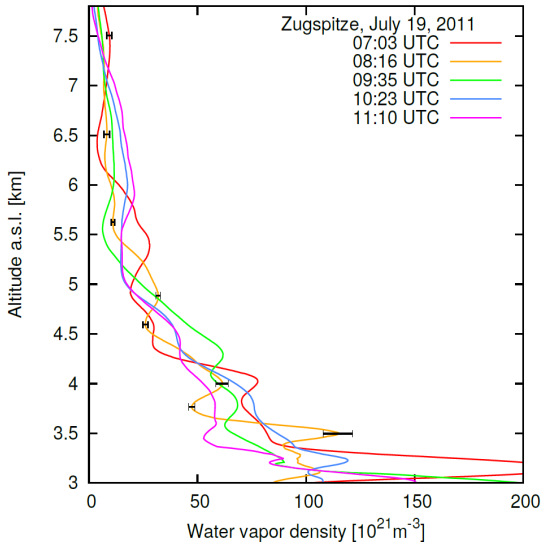

Figure 9: Short-term variability of the water vapor profile induced by convection under atmospheric instability, high-reaching convection, and only a few hours before the formation of a thunderstorm. The example error bars (+- 2σ) represent statistical uncertainties caused by electronic noise in the detection.

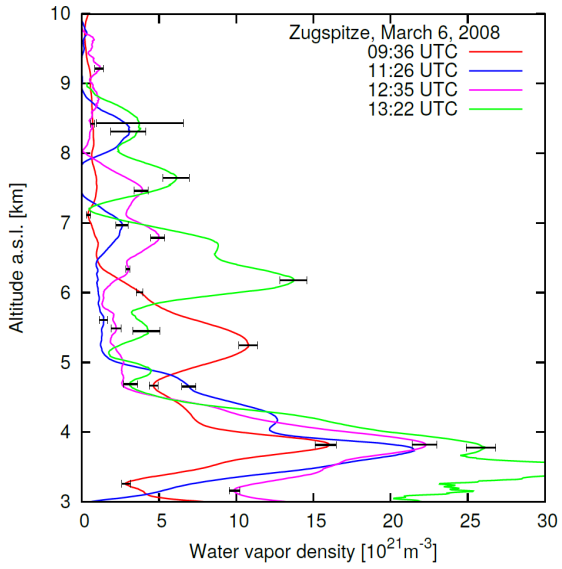

Figure 10: Example of extreme temporal variability of the vertical distribution of water vapor during a stratospheric intrusion event. Due to the advection velocity of about 11 m/s at an altitude between 3 km and 4 km (data from radiosonde at Munich at 12h UTC, 100 km to the north), a time shift of 1 hour corresponds to a horizontal shift of about 40 km within this altitude range. The example error bars (+- 2σ) represent statistical uncertainties caused by electronic noise in the detection.

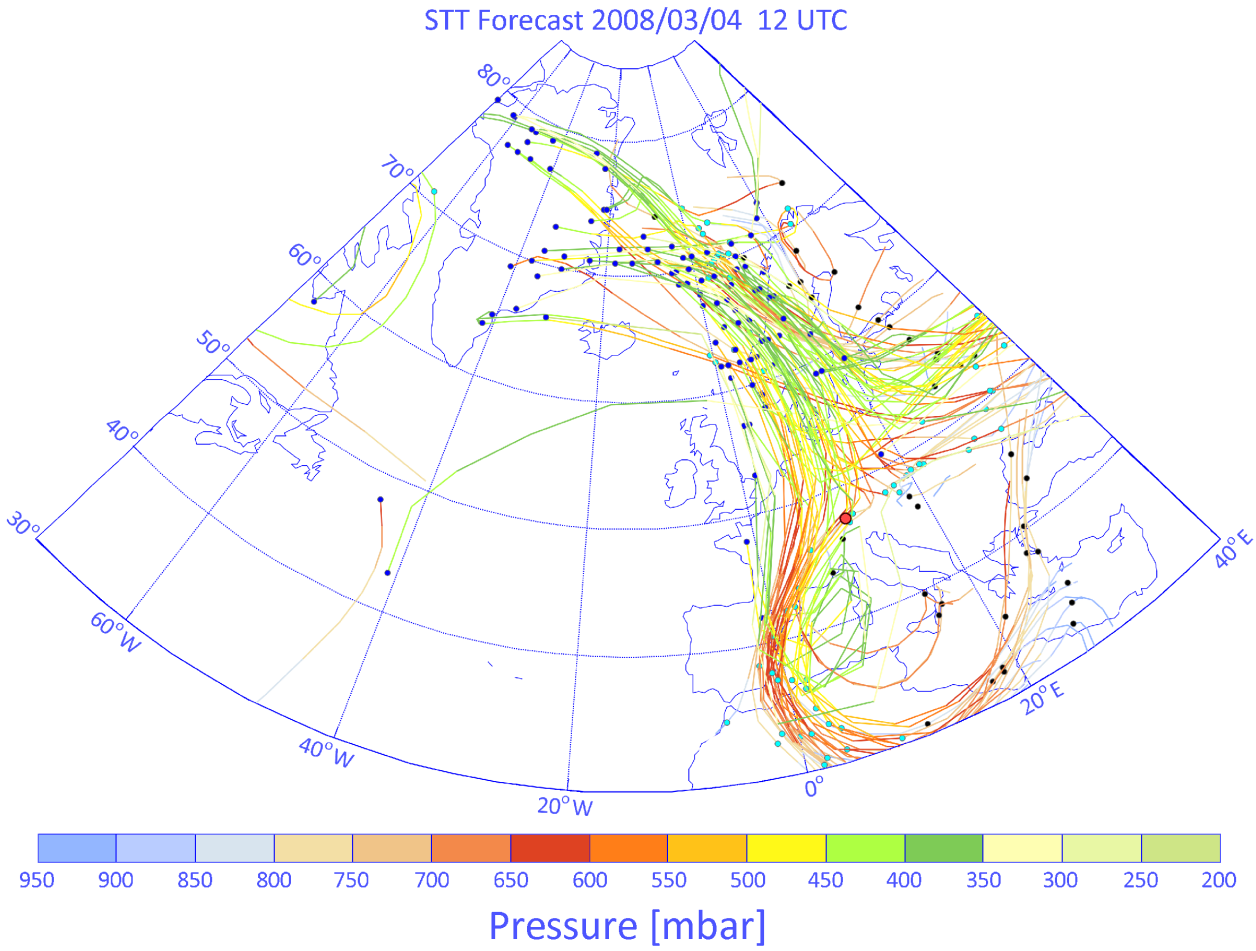

Figure. 11: Four-day forward trajectories by ETH Zürich for a stratospheric intrusion in early March 2008. The red point marks the location of the Zugspitze site (47.42°N, 10.98°E). The trajectories start two days in advance (dark blue points) to the case illustrated in Fig. 10. The colors indicate the air pressure along their path. They show several limbs of stratospheric air descending from Greenland and hitting the location of Mt. Zugspitze at different altitudes (different colors) at the same time on March 6, 2008. This trajectory plot was taken from our recent publication which describes this case in much more detail (Trickl et al., 2014).

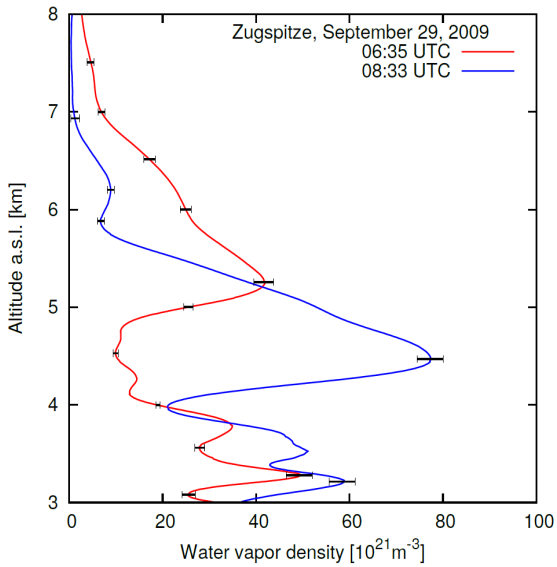

Figure 1~~1~~2: Example of extreme temporal variability of the vertical distribution of water vapor under rather humid conditions. Due to a wind speed of about 16 m/s at an altitude of 4.5 km (data from radiosonde Munich at 12:00 UTC, 100 km to the north), a time shift of 2 hours corresponds to a horizontal shift of about 115 km at this altitude. The two profiles were recorded within less than two hours. The example error bars (+- 2σ) represent statistical uncertainties caused by electronic noise in the detection.

30

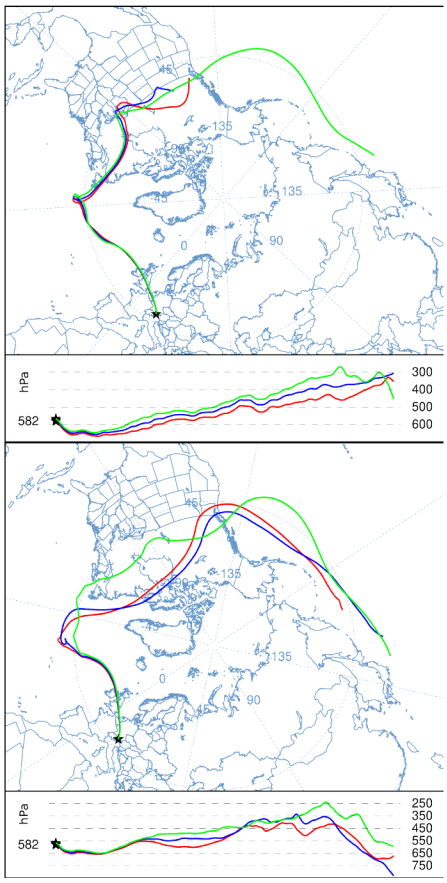

Figure 12: Backward trajectories from the NOAA HYSPLIT model (see text) ending above Mt. Zugspitze at 4600m, 4700m and 4800m a.s.l. at 6:00 UTC (upper plot) and 8:00 UTC (lower plot), July 29, 2009 were calculated from reanalysis data with a vertical velocity model and a duration of 315 hours. The vertical sections are referred to the air pressure along the pathways. The remarkable coherence of the three pathways during a longer time indicates a rather good reliability.

Page : 3 Line : 116 Author : Hannes Vogelmann 02/09/2015
Refers to Referee #2, comment 2.

Page : 3 Line : 134 Author : Hannes Vogelmann 02/02/2015
Refers to Referee #2, comment 4.

Page : 4 Line : 159 Author : Hannes Vogelmann 03/03/2015
Added due to comment T4, Referee #1.

Page : 5 Line : 183 Author : Hannes Vogelmann 03/02/2015
Added to makes things more clear, due to comment 1, Referee #2

Page : 5 Line : 196 Author : Hannes Vogelmann 02/09/2015
Added equations and text due to comment 1 by Referee # 2.

Page : 5 Line : 201 Author : Hannes Vogelmann 03/02/2015
Added information about uncertainty and reliability in context with the sample size, as requested by Referee #1, comment 1.

Page : 5 Line : 204 Author : Hannes Vogelmann 03/02/2015
Added comment about instrument integration times as requested by comment s1, Referee# 1

Page : 6 Line : 217 Author : Hannes Vogelmann 03/02/2015
Sentence and References added due to comment s2, Referee #1.

Page : 6 Line : 252 Author : Hannes Vogelmann 03/02/2015
Modiefied due to comment s4, Referee #1.

Page : 6 Line : 255 Author : Hannes Vogelmann 03/02/2015
Sentence added due to comment s4, Referee #1.

Page : 9 Line : 366 Author : Hannes Vogelmann 03/03/2015
Added due to comment 3, Referee #1.

Page : 9 Line : 372 Author : Hannes Vogelmann 03/03/2015
Added due to comment 5, Referee #2.

Page : 10 Line : 406 Author : Hannes Vogelmann 03/03/2015
Added due to comment t2, Referee #2.

Page : 10 Line : 425 Author : Hannes Vogelmann 02/25/2015
Refers to comment 3, Referee #1.

Page : 11 Line : 452 Author : Hannes Vogelmann 02/25/2015
Refers to comment 3, Referee #1

Page : 11 Line : 464 Author : Hannes Vogelmann 02/25/2015
Refers to comment 3, Referee #1

Page : 13 Line : 547 Author : Hannes Vogelmann 02/25/2015
Refers to comment 2, Referee #1.

Page : 18 Line : 788 Author : Hannes Vogelmann 03/06/2015
Reference added, due to model used for the trajectory plot in new Fig. 11

Page : 19 Line : 815 Author : Hannes Vogelmann 02/09/2015
Added due to Referee #2, comment 2.

Page : 21 Line : 828 Author : Hannes Vogelmann 02/02/2015
Error bars added due to comment 1 of Referee #1.

Page : 21 Line : 836 Author : Hannes Vogelmann 02/09/2015
Refers to Referee #2, comment 3.

Page : 22 Line : 847 Author : Hannes Vogelmann 02/02/2015
Error bars added due to comment 1 of Referee #1.

Page : 23 Line : 866 Author : Hannes Vogelmann 02/02/2015
Error bars added due to comment 1 of Referee #1.

Page : 26 Line : 898 Author : Hannes Vogelmann 02/02/2015
Error bars added due to comment 4 of Referee #2.

Page : 27 Line : 916 Author : Hannes Vogelmann 02/02/2015
Error bars added due to comment 4 of Referee #2.

Page : 28 Line : 937 Author : Hannes Vogelmann 02/02/2015
Error bars added due to comment 4 of Referee #2.

Page : 29 Line : 957 Author : Hannes Vogelmann 02/25/2015
Added Figure as suggested by comment 3, Referee #1.

Page : 30 Line : 967 Author : Hannes Vogelmann 02/02/2015
Error bars added due to comment 4 of Referee #2.

Page : 31 Line : 1016 Author : Hannes Vogelmann 02/25/2015
Added Figure as suggested by comment 3, Referee #1,Last sentence refers to comment 5, Referee #2.